Correlated Electrical and Optical Studies of Hybrid Argon Gas–Water Plasmas and their Application to Tooth Whitening

Myoung Soo Kim, Il Gyo Koo,* Myeong Yeol Choi, Jae-Chul Jung, Fathala Eldali, Jae Koo Lee, George J. Collins

Radio frequency (RF) driven hybrid gas–water plasma for tooth whitening was developed and the plasma chemical reactions with de-ionized (DI) water were studied. Plasma operating conditions, such as RF input power and argon flow rate were correlated with plasma lengths. The operation of hybrid gas–water plasma changed both the electrical conductivity and pH concentration of the DI water. OH and H_2O_2 densities were measured to determine the dominant species generated by plasma. The major chemical reaction pathways and known rate constants are given in support of the analysis of major chemical reaction pathways. Finally, we demonstrated that the hybrid gas–water configuration achieved porcine tooth whitening.

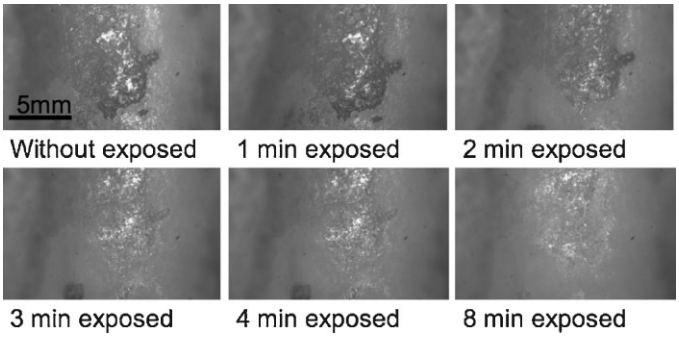

1. Introduction

Cold atmospheric plasmas have been employed for dental applications,[1,2] sterilization,[3,4] cancer treatment,[5,6] tissue removal[7–9] and a means of changing chemical composition of feedstock gases.[10] The UV and ions generated by atmospheric plasma, as well as OH, O, H, NO, and O_3 reactive species drive these applications.[11] Tooth whitening by plasma treatment is one of such applications that require high rates of chemical reaction and low gas temperature since the gum tissue surrounding teeth is not as robust as the teeth at over 60 °C. For example, Lee el al. achieved tooth whitening primarily by employing the OH radicals from either pure water or a H_2O_2 containing solution, which was poured on the tooth surface, while simultaneously excited by helium gas plasma.[1] There are prior studies of the plasma characteristics and their effect on the liquid conductivity and pH,[12–15] as well as on the antibacterial effects.[16] We show here that the hybrid gas–water plasma can achieve both high rates of chemistry on tooth surfaces and maintain low ambient temperature on nearby soft tissue. Hybrid gas–water plasmas can balance requirements of high fluxes of photons and radicals with low ambient temperatures. The surface of treated tissue was not directly affected by hybrid gas–water plasmas because the plasma was surrounded by water. We present major chemical reaction pathways between water lying mm to cm away from the plasma jet injection location. These pathways analysis are based on both measurements of optical emission from the plasma jet and simultaneously measured chemical changes in the liquid environment.

M. S. Kim, Dr. I. G. Koo, J. K. Lee
Department of Electrical Engineering, Pohang University of Science and Technology, Pohang 790-784, Republic of Korea
Fax: +1 970 491 8671; E-mail: ilgyokoo@engr.colostate.edu
Dr. I. G. Koo, M. Y. Choi, J.-C. Jung, F. Eldali, G. J. Collins
Department of Electrical and Computer Engineering, Colorado State University, Fort Collins, Colorado 80523, USA

DOI: 10.1002/ppap.201100141

The chemical reaction rates indicated that the main change is in the concentrations of de-ionized (DI) water electrical conductivity and pH. Subsequent reactions changed the OH and H_2O_2 reactive species. Finally, we present data obtained from both optical and scanning electron microscope (SEM) measurements regarding optimized plasma plume length versus injected gas flow rate and applied power. These observations were used to determine the optimum placement of tooth/tissue samples to be irradiated. The range of optimal electrode locations was found to be 3–15 mm away from the water surface, which allows a tradeoff between ambient temperature at the surface of teeth and total flux of radicals impinging on the tooth surface.

2. Experimental Section

2.1. Plasma Treatments

A 13.56 MHz power supply Advanced Energy, CESAR RF power generator was connected to the hybrid gas–water plasma system through a matching box. The coaxial plasma electrode consisted of an external insulating ceramic tube and the inner metallic electrode covered by a ceramic tube, as shown in Figure 1. The argon gas was injected through the stainless steel tube into DI water. The argon gas flow rate was controlled by a mass flow controller (Aera, TC FC-PA780c) and a digital flow controller (Advanced Energy, ROD-4). The initial electrical conductivity DI water was less than 0.5 $\mu S \cdot cm^{-1}$. The electrode tip was soaked 1.5 cm deep from the surface of the DI water.

2.2. Plasma Characteristics Measurements

Optical methods were employed to measure plasma characteristics. Plasma length in the water was measured with a CCD camera (Princeton instruments, 7467-0028). We made three independent plume length measurements of argon plasma jets based on total optical emission, at each plasma condition and took the average value of the readings. The spectrally resolved emission from the gas–liquid hybrid plasma was measured with a spectrometer (Princeton instrument/ACTON, spectropro2750). The spectral data

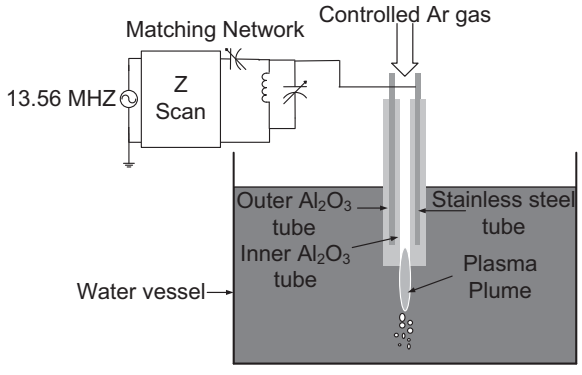

Figure 1. Schematic of the experimental setup and electrode configuration for creating hybrid gas/liquid plasmas.

was used to estimate OH and H_2O_2 concentrations as a function of the treatment time. The plasma gas temperature in the water was estimated by comparing the OH spectrum with simulation results of a LIFbase simulation program.

2.3. Measurement of DI Water Changes versus Plasma Jet Conditions

To analyze the effect of the plasma on DI water, we measured the changes of the electrical conductivity, the pH, the temperature, and concentrations of the hydrogen peroxide (H_2O_2), and hydroxyl (OH) radicals. Two or more 100 mL DI water samples were prepared for every single characteristic measurement of plasma treated DI water. The baseline conditions in DI water were measured for one of the samples without any plasma treatment and the other was measured after the plasma treatment. The experiments were conducted four times for each of the six plasma exposure times.

The conductivity, pH, and temperature measurements were measured with three separate sensors: Thermo fisher scientific 013605MD, 8102BNUWP, 927006MD, respectively, for 5, 10, 15, 20, 30 and 60 min of plasma treatment time. The H_2O_2 concentration in DI water was measured with a chemical assay kit (Cayman chemical company, Hydrogen peroxide assay kit, Catalog No. 706001). The absorbance of 666.02 nm light of methylene blue (MB) solution was recorded to measure the change in OH radical concentration after the plasma treatment. We prepared five standard concentration of MB solution from 25.4 to 1.27 μM and made a calibration curve using UV absorption spectroscopy. The concentration of OH radicals was measured by comparing the absorbance of plasma treated DI water with an untreated reference solution absorbance. In our results and discussion analysis given below, we choose only the saturated value of all measurements taken and the effect of DI water temperature on these values was compensated.

2.4. Teeth Sample Preparation and Analysis

Naturally stained porcine teeth were supplied from the Colorado State University Veterinary School. The teeth were placed 3–15 mm away from the electrode and exposed to the argon plasma in DI water. This allowed for the plasma plume to spread out over the entire tooth surface and to provide a low ambient surface temperature. The surface color changes were characterized using CCD camera system. Plasma treated tooth surface topography was quantified by SEM image, after 10 min of plasma exposure.

3. Results and Discussion

3.1. Plasma Conditions

The plasma length in DI water has a limited range of penetration and a limited geometric stability. The stability depends primarily on two experimental parameters: level of applied RF power and argon gas flow rate. The plume lengths of the plasma versus applied RF power and gas flow rate were given in Figure 2 and 3, respectively. No penetration of the jet into DI water occurred when using

DOI: 10.1002/ppap.201100141

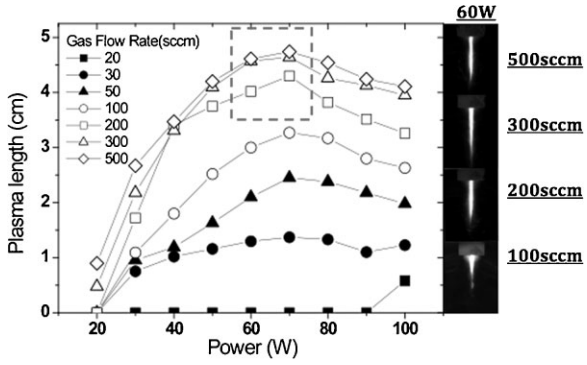

Figure 2. Plasma plume length injected into water, as measured by total optical emission as a function of the applied RF power. Each line corresponds to one gas flow rate. The red box is optimal points according to the plum length saturation. The side pictures are comparing the plume lengths measured at 60 W. The gas flow is 100, 200, 300 and 500 sccm from bottom to the top.

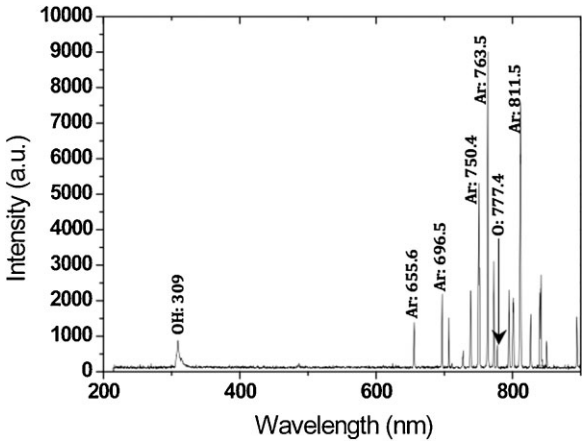

Figure 4. Typical optical emission spectrum from a glow discharge in hybrid gas/liquid plasma.

less than 50 sccm argon gas flow rate. The plasma expanded into the water at 100–500 sccm. The plasma length was not repeatable at a flow rates over 400 sccm. Therefore, the stable argon gas flow rate into DI water for repeatable experiment was between 50 and 400 sccm. This limited flow rate window was chosen for all experimental conditions. Plasma length measurements were repeated three times to determine the average plasma plume length under each experimental condition taking into account the desired set of conditions at the tooth surface. Fortunately, under these hydrodynamic conditions, the plume length increases monotonically with the applied RF power to reach an optimal point as indicated in Figure 2.

3.2. Plasma Temperature Measurements

Figure 4 shows the Ar, H, O and OH emission lines of the plasma between 200 and 850 nm.[12] The discharge emission did not show any characteristic lines for nitrogen atoms or molecules in contrast with strong O emission lines. The experimental OH spectrum was observed and compared with the simulated band of OH as shown in Figure 5. The rotational temperature from OH spectrum was estimated by fitting the experimental spectrum to the LIFbase simulated spectrum.[17] The temperature of the plasma gas can be approximated by the rotational temperature under high pressure conditions. The estimated rotational temperature was about 2 000 K in the core of the plasma jet at 60 W applied RF power and 250 sccm gas flow rate. The gas temperature of the argon gas plasma jet varies sharply with the spatial position, as it is rapidly cooled down by the surrounding DI water. Water temperature at about 3 mm below the plasma termination position was 35 ± 5 °C, as measured by optical thermal probe.

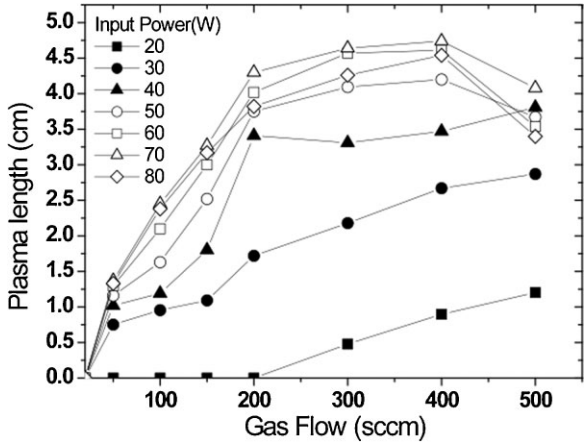

Figure 3. Plasma plume length injected into water, as measured by total optical emission as a function of argon gas flow rate.

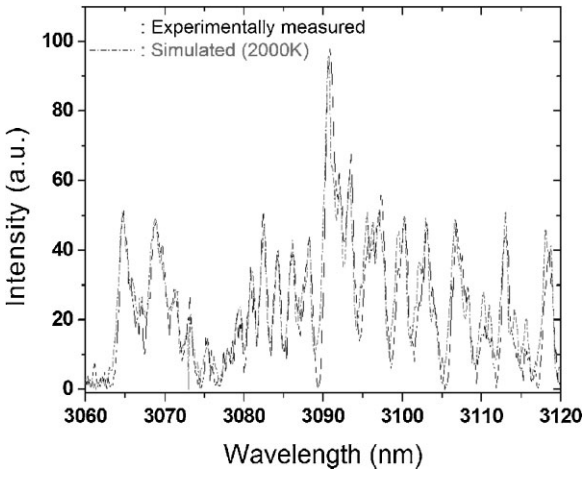

Figure 5. Comparison of both measured OH band spectra and simulated spectra (LIFbase) for the determination of the rotational temperature of hybrid plasma at 60 W RF input power.

3.3. Plasma Chemical Reactions in DI Water

Our aim was to better understand the chemistry between the argon plasma and DI water. We observed and correlated the changes in the DI water properties such as: pH, electrical conductivity, dissolved OH radicals and hydrogen peroxide densities. The test conditions for these observations were kept at 250 sccm of argon and 60 W of input power, since the pH of DI water changes with plasma conditions. Figure 6 shows the pH of DI water versus the plasma treatment time. The pH values of DI water decreased with increasing time and finally saturated at 4.6. Figure 6 also contains the gas only treated line. The effect of argon gas flow only was measured for 60 min. When compared with gas only treated results, it is clear that the change in pH cannot be attributed to the argon gas, but to the plasma. As seen in Figure 7, the electrical conductivity of DI water increased linearly with increasing the argon plasma exposure time. The value of the DI water exposed to argon gas without the plasma was also included in Figure 7. The conductivity changes of the DI water have possible contributions from the ions which are obtained from H_2O molecule, such as: H_3O^+, H^+, OH^- and O_2^-.[18] Electrical conductivity can be obtained from the pH in Figure 6 by assuming that the positive ions are hydrogen ions, H^+, and that the negative ions are electrons.

Electrical conductivity can be calculated using:

$$\sigma = -\rho_e \mu_e + \rho_h \mu_h \quad (1)$$

In Equation (1), the charge density and mobility are expressed by $\rho_e(\rho_h)$ and $\mu_e(\mu_h)$, respectively, with notation for electron and hole. The charge density of hydrogen is equal to its mol concentration × Avogadro's number × Coulomb number/100 mL ($Q \cdot m^{-3}$). The mol concentration of hydrogen ion was taken from the measured pH value. The conductivity change due to H^+ ions is calculated by multiplying the mobility of hydrogen ion 36.23×10^{-8} ($m^2 \cdot s^{-1} \cdot V^{-1}$) with the charge density.[19] The calculated conductivity from the hydrogen concentration is compared with measured conductivity in Figure 7. Note that every calculated conductivity well comply with the measured electrical conductivities. The small differences observed between measured and calculated conductivities are, in our opinion, due to other ions generated in the solution from secondary reactions. For example, the negative OH ions could be generated from the gas phase OH molecules and subsequently dissolved into DI water as OH^-. Next, we looked at the major chemical reaction pathways in the hybrid gas–water plasma. The OH radicals and H_2O_2 in DI water are the two major reactive chemical species created by the plasma jets. The measured concentrations of OH

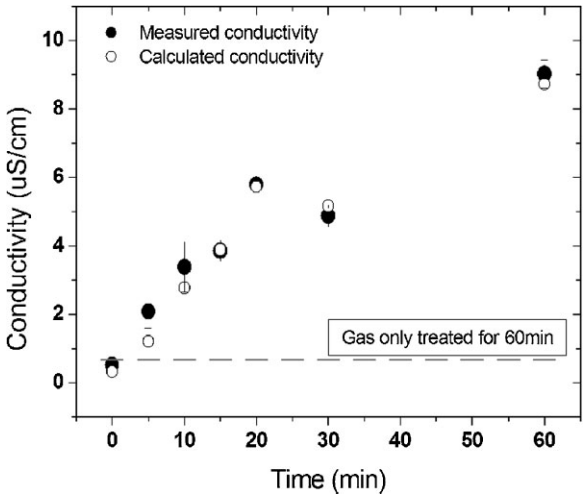

Figure 7. Comparison of measured conductivity (solid dot) and calculated conductivity (open dot) versus plasma treatment time.

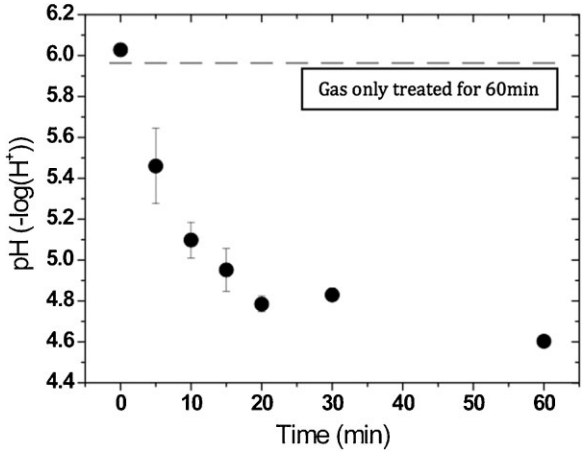

Figure 6. The pH change of plasma treated DI water versus plasma treatment time. The dashed line is for unexcited neutral argon gas bubbling.

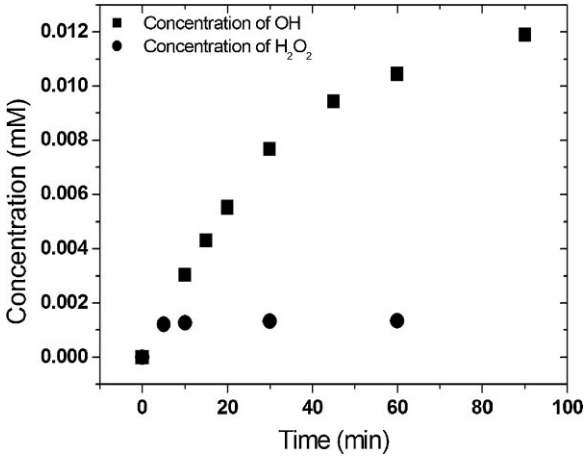

Figure 8. The concentrations of both OH (rectangle dots) and H_2O_2 (circled dots) versus plasma treatment time.

DOI: 10.1002/ppap.201100141

and H_2O_2 molecules are shown in Figure 8. The OH concentration is measured to be of order of 10^{-5} mole and increases with increasing the treatment time, while the concentration of H_2O_2 plateaus at order of 10^{-6} mole. Therefore, OH generation in the gas phase contributes to the liquid phase concentration change via the following reaction sequences:

$$e + H_2O \rightarrow H^+ + OH^- + e \quad (2)$$

$$e + H_2O \rightarrow O + H_2^+ + 2e \quad (3)$$

$$2OH \rightarrow H_2O_2 \quad (4)$$

$$OH^- + O \rightarrow HO_2 + e \quad (5)$$

The OH^- ions are generated as primary species from the decomposition of the H_2O molecules. H_2O_2 and HO_2 are generated via reactions which are consequent to OH^- generation. Below there is a list of well-known rate constants based on refs.[8,20]

HO_2 Generation reaction Rate Coefficient $(cm^3 \cdot s^{-1})$

$$e + H_2O_2 \rightarrow H + HO_2 + e \quad 3.1E\text{-}11 \quad (6)$$

$$OH^- + O \rightarrow HO_2 + e \quad 2E\text{-}10 \quad (7)$$

H_2O_2 Generation

$$2HO_2 \rightarrow H_2O_2 + O_2 \quad 1.15E\text{-}11 \quad (8)$$

$$2OH \rightarrow H_2O_2 \quad 1.1253E\text{-}12 \quad (9)$$

OH Generation

$$e + HO_2 \rightarrow OH + O + e \quad 1.67E\text{-}09 \quad (10)$$

$$e + H_2O_2 \rightarrow 2OH + e \quad 2.36E\text{-}09 \quad (11)$$

From the published rate coefficients, simple equilibrium kinetics indicates that the conversion of other species to the OH is higher than the opposite reactions by factors of 10–100. This corresponds to the saturated regions of our data, and is consistent with Figure 8. For H_2O_2, the generation rate (Reaction 8 and 9) is much less than the conversion rate for H_2O_2 (Reaction 11). This species should remain at very low concentrations, as supported by the results in Figure 8. The exchange between H_2O_2 and HO_2, is described in Equation (2 and 4). The rate coefficients of them are of the same order of magnitude.

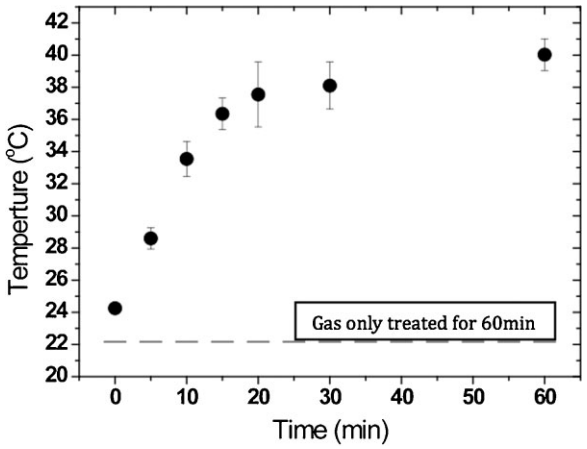

Figure 9. The temperature of plasma treated DI water versus plasma treatment time. The temperature does not exceeded 40 °C even after 60 min of plasma treatment.

Therefore, we think that the OH molecules are the dominant species in the hybrid argon gas–liquid plasma producing either OH radicals in the gas phase or OH^- ions in DI solutions. The actual reactions in plasma–liquid interface are expected to be more complicated than those described in this paper. Further research needs to be done for a more reliable reaction analysis.

3.4. Tooth Whitening Using RF Argon-DI Water Hybrid Plasmas

From our studies above, the hybrid plasma generates primarily OH radicals and H_2O_2 molecules. It is believed that the OH species can promote chemical pathways useful for tooth whitening. Therefore, the hybrid argon gas–liquid plasma can be a candidate for the tooth whitening application. We also measured very low concentration (<0.03 wt.-%) of H_2O_2 in DI water. Low concentration of H_2O_2 (<30 mM), as detailed in ref.,[21] will not induce cell

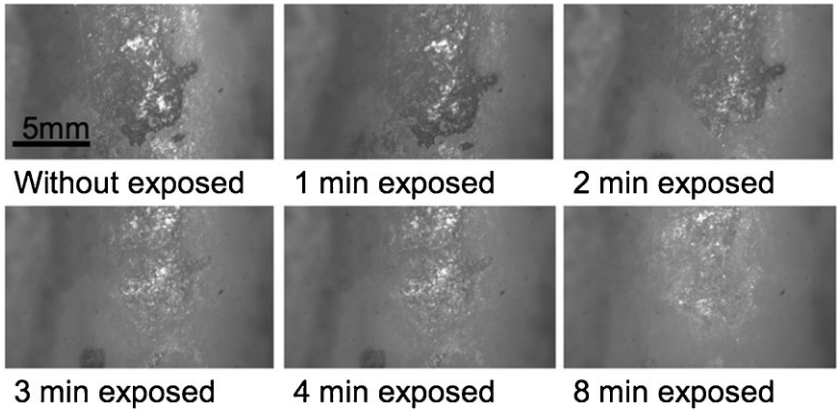

Figure 10. The surface color change of the tooth versus plasma treatment time.

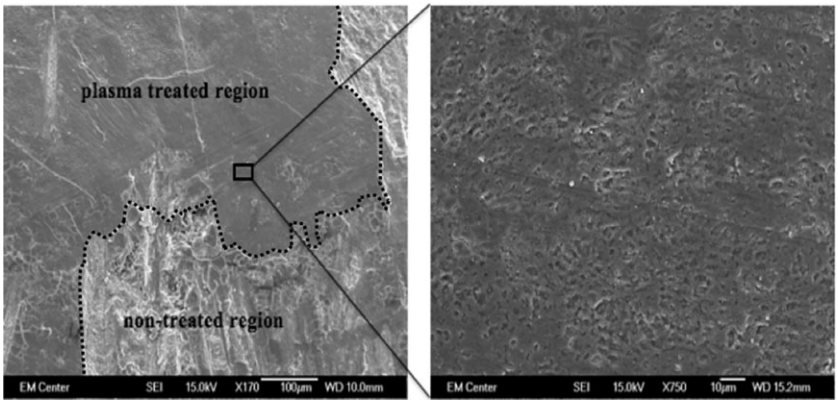

Figure 11. The SEM images of the tooth surface after hybrid plasma exposure for 10 min: low magnification (×170) on the left and high magnification (×750) on the treatment side.

death to the surrounding soft tissue. Soft tissue damage was negligible when treated at a greater distance than 3 mm measured from the end of the plasma plum. The temperature of the plasma treated DI water never exceeded 40 °C, as shown in Figure 9. The effect of the hybrid plasma on the irradiated tooth surface versus exposure time is shown in Figure 10. The entire tooth stain was removed within 10 min by hybrid plasma treatment. To confirm low damage levels on the enamel, the SEM pictures in Figure 11 indicated that the plasma removed stain material from the enamel, without inducing surface defects on the enamel.[22]

4. Conclusion

RF Ar-DI water hybrid plasmas were investigated by optical, electrical, and chemical means as a function of the plasma treatment duration. We found that the measured electrical conductivity increased as a result of the plasma treatment, and was correlated with the measured decreasing pH value. It supports that both hydrogen peroxide and hydroxyl radicals are generated from the collision between energetic electrons and water molecules. The primary and secondary reaction pathways underlying these observations agreed with the measurements of high OH densities and low H_2O_2 densities. Hence, it was confirmed by both optical and SEM studies that tooth whitening by the hybrid gas–liquid plasma was driven primarily by OH radicals. We speculate that RF gas–liquid plasma configurations and choices of feedstock liquids and gases can be tailored for specific chemistries for other biomedical applications.

Acknowledgements: This work was supported by Mid-career Researcher Program through NRF grant funded by the Korea MEST (2011-0015395) and Bioscience Discovery Evaluation Grant Program of the Colorado State Government (10BGF-25). The grant funded by the Korean government and Korea Ministry of Education, Science and Technology was through its Brain Korea 21 program. All authors are thankful for the contributions of Dr. Hyun Woo Lee at the Pohang University of Science and Technology who developed the simulation programs.

Received: July 12, 2011; Revised: October 26, 2011; Accepted: October 28, 2011; DOI: 10.1002/ppap.201100141

Keywords: atmospheric pressure plasmas; chemical; liquid plasmas; reactions; tooth whitening

[1] H. W. Lee, G. J. Kim, J. M. Kim, J. K. Park, K. Lee, G. C. Kim, *J. Endod.* **2009**, *35*, 587.
[2] X. Lu, Y. Cao, P. Yang, Q. Xiong, Z. Xiong, Y. Xian, Y. Pan, *IEEE Trans. Plasma Sci.* **2009**, *37*, 5.
[3] C. Jiang, M. T. Chen, C. Schaudinn, A. Gorur, P. T. Vernier, J. W. Costerton, D. E. Jaramillo, P. P. Sedghizadeh, M. A. Gundersen, *IEEE Trans. Plasma Sci.* **2009**, *37*, 7.
[4] M. Laroussi, *Plasma Process. Polym.* **2005**, *5*, 391.
[5] G. C. Kim, G. J. Kim, S. R. Park, S. M. Jeon, H. J. Seo, F. Iza, J. K. Lee, *J. Phys. D: Appl. Phys.* **2009**, *42*, 032005.
[6] G. Fridman, A. Schereshevsky, M. M. Jost, A. D. Brooks, A. Fridman, A. Gutsol, V. Vasilets, G. Fridman, *Plasma Chem. Plasma Processes* **2007**, *27*, 163.
[7] K. R. Stalder, J. Woloszko, I. G. Brown, C. D. Smith, *Appl. Phys. Lett.* **2011**, *79*, 27.
[8] D. V. Palanker, A. Vankov, P. Huie, *IEEE Trans. Biomed. Eng.* **2009**, *55*, 2.
[9] I. G. Koo, C. A. Moore, M. Y. Choi, G. J. Kim, P. Y. Kim, Y. S. Kim, Z. Yu, G. J. Collins, *Plasma. Process. Polym.* **2011**, *8*, 1103.
[10] I. G. Koo, M. S. Lee, J. H. Shim, J. H. Ahn, W. M. Lee, *J. Mater. Chem.* **2005**, *15*, 4125.
[11] A. Rahman, A. P. Yalin, V. Surla, O. Stan, K. Hoshimiya, Z. Yu, E. Littlefield, G. J. Collins, *Plasma Sources Sci. Technol.* **2004**, *13*, 537.
[12] H. Aoki, K. Kitano, S. Hamaguchi, *Plasma Sources Sci. Technol.* **2008**, *17*, 025006.
[13] T. Maehara, S. Honda, C. Inokuchi, M. Kuramoto, S. Mukasa, H. Toyota, S. Nomura, A. Kawashima, *Plasma Sources Sci. Technol.* **2011**, *29*, 034016.
[14] M. Sato, T. Ohgiyama, J. S. Clements, *IEEE Trans. Ind. Appl.* **1996**, *32*, 106.
[15] T. Kaneko, K. Baba, T. Harada, R. Hatakeyama, *Plasma Process. Polym.* **2009**, *6*, 713.
[16] F. Liu, P. Sun, N. Bai, Y. Tian, H. Zhou, S. Wei, Y. Zhou, J. Zhang, W. Zhu, K. Becker, J. Fang, *Plasma Process. Polym.* **2010**, *7*, 231.
[17] LIFBASE: *Database and Spectral Simulation Program version 2.0.64*, SRI international report MP99- 009, http://www.sri.com/cem/lifbase (**1999**).

DOI: 10.1002/ppap.201100141

[18] I. G. Koo, W. M. Lee, *Jpn. J. Appl. Phys.* **2006**, *45*, 10A.
[19] P. W. Atkins, *Physical Chemistry*, 6th ed., John Wiley & Sons, New York, USA **1998**, p. 740.
[20] D. X. Liu, P. Bruggeman, F. Iza, M. Z. Rong, M. G. Kong, *Plasma Sources Sci. Technol.* **2010**, *19*, 025018.
[21] E. R. Whittemore, D. T. Loo, J. A. Watts, C. W. Cotman, *Neuroscience* **1995**, *61*, 4.
[22] Y. C. Chiang, B. S. Lee, Y. L. Wang, Y. A. Cheng, Y. L. Chen, J. S. Shiau, D. M. Wang, C. P. Lin, *Lasers Med. Sci.* **2008**, *23*, 41.